Turkish Journal of Electrical Engineering & Computer Sciences

http://journals.tubitak.gov.tr/elektrik/

Research Article

Turk J Elec Eng & Comp Sci
(2020) 28: 1503 – 1518

doi:10.3906/elk-1908-179

Analysis of condition number and position estimation error for multiangulation position estimation system

Sa'id Musa YARIMA[1,2,*], **Ahmad Zuri SHA'AMERI**[1], **Abdulmalik Shehu YARO**[3]

[1]Division of Electronic and Computer Engineering, Faculty of Engineering, Universiti Teknologi Malaysia, Johor, Malaysia

[2]Department of Electrical and Electronics Engineering, Abubakar Tafawa Balewa University, Bauchi, Nigeria

[3]Department of Electronics and Telecommunications Engineering, Ahmadu Bello University, Zaria, Nigeria

Received: 31.08.2019 • **Accepted/Published Online:** 20.01.2020 • **Final Version:** 08.05.2020

Abstract: A passive wireless positioning system could be used to detect the location of low-level airborne targets such as drones or unmanned aircraft systems from the electromagnetic emission detected at spatially deployed ground receiving stations (GRSs). The multiangulation system proposed in this paper makes use of the angle of arrival (AOA) of the transmitted signal from the target to estimate its position through a 2-stage process. The AOA is the position-dependent signal parameter (PDSP) obtained from the target emission in the first stage, and using the PDSP and GRSs, the target location is estimated in the second stage by the angulation algorithm. Noise in the received signal results in AOA estimation error and subsequently error in the position estimation (PE). This paper focuses on the angulation process, which is the second stage of the multiangulation target location estimation process. Analysis is conducted to determine the correlation between the PE error and the condition number of the coefficient matrix of a multiangulation position estimation system. The results based on Monte Carlo simulations show that both condition number and PE error distribution increase with the target range, where the higher condition number values correlate with higher PE error values appearing around 80° to 110° and 260° to 280° of both distributions.

Key words: Angle of arrival, free-space path loss, singular-value decomposition, position estimation

1. Introduction

Position estimation (PE) of aircraft such as drones, attack helicopters, and fighter jets is one of the fundamental functions of electronic warfare (EW) and plays a vital role in defense strategy, security, and anti-hostile actions [1]. EW is used by the military to control the electromagnetic spectrum in order to attack or impede enemy assaults. Its broad coverage falls in three main subdivisions: electronic support (ES), electronic attack (EA), and electronic protection (EP) [2–4]. Among this division, ES performs such tasks as characterization or detection of signals used by the aircraft referred to as spectrum surveillance, a technique that records, processes, and evaluates recorded spectrum data [5]. For government regulatory bodies such as the Federal Communications Commission (FCC) and the Malaysian Communications and Multimedia Commission (MCMC), the main purpose is to regulate the activities of spectrum users [6]. Signals of interest in spectrum surveillance could be radar or communications signals [7].

Radar is the common technology for aircraft surveillance. A number of limitations such as susceptibility to EA and difficulty to detect low-altitude targets [8], however, compromise some of radar's functions in both

*Correspondence: saeedmusayarima@gmail.com

civilian and military surveillance applications. Passive PE systems like MPE systems based on the angle of arrival (AOA) of the signal and multilateration (MLAT) based on time difference of arrival (TDOA) could complement radar in PE of aircrafts [9]. While the former uses an angulation algorithm to determine the PE, the later woks with a lateration algorithm to compute the PE. Both methods are implemented as a two-stage process that involves first determining the PDSP and the use of the PDSP to perform PE [10, 11]. MLAT can perform PE in 2D with a minimum of three GRS sensors and with more sensors it can perform 3D PE [12]. The major constraint in all time-based PE techniques like MLAT is the critical clock synchronization requirement [13], as reported in [14]. Comparisons were made in [14, 15] between AOA and TDOA methods. It was, in general, reported that AOA methods require fewer receivers and higher reliability of data backhaul and bandwidth. The TDOA performance is bandwidth-dependent and it is difficult to locate slowly varying signals like unmodulated carriers. It therefore becomes poorer with decreasing signal bandwidth while the AOA technique has the advantage of performing PE in those conditions. On the other hand, the receive-signal strength (RSS)-based method is highly unpredictable due to delayed multipaths and is generally restricted to indoor deployments [16, 17].

A performance evaluation based on a four-GRS square layout was done in [9] for low-level airborne targets. Comparisons made between MLAT and MPE systems showed that MLAT had lower root mean square error (RMSE) than the MPE system within a target range of less than 30 km on the horizontal plane while the MPE showed better RMSE performance at ranges between 30 km and 50 km. Similar GRS arrangement was used in [17], which proposed PE using an AOA-based estimator for sectorized antennas with n sensors and 50 random GRS positions. Increasing the number of sensors from 4 to 16 increased both the AOA and the probability of the algorithm for correct PE measurement between 75% and 85%.

The main objective of this research is to investigate the correlation that exists between the coefficient matrix condition number and the position estimation error (PE). The remainder of this paper is organized as follows: In Section 2, we describe the function of ES in a positioning system with subsections covering the problem, angulation algorithm, and angulation algorithm PE. Section 3 describes the PE error analysis while Section 4 presents the simulation results including estimation of AOA error standard deviation and analysis of PE error and condition number.

2. Overview of ES system

EW involves monitoring of the electromagnetic (EM) spectrum and use of the directed energy to control the spectrum, usually to protect a friendly platform and inflict an attack on an adversary [2–4]. The ES system works by intercepting and acquiring the enemy's radiated energy, which may be emitted from communication networks, radars, telemetry transmitters, or unintended radiation from computer clocks [8, 18]. Its main objective is to acquire intelligence features derived from the adversary's radiation such as position, identity, and degradation of the radar or communication systems' performance by using a random noise jammer or coherent smart jammers [3, 8].

The basic functions in the ES system are divided into two parts [19]: target locating and signal processing, which includes the signal reception, signal analysis and classification, decision-making, and signal database. The target locating part determines the location of the radiating source by employing the RSS, AOA, or TDOA methods [1, 9]. At the signal processing level, the frequency components of the down-converted signals are detected and the signals present at the detected frequency are then classified based on the modulation type.

This is followed by the parameter estimation, whose output is fed to the classifier to resolve the identity of the signal. Finally, the signal database is updated or appropriate countermeasures such as radiofrequency countermeasures or radar jamming and deception are applied [2, 20]. It is important to note that the structure of ES described here is implemented in a single GRS and can only resolve the AOA of the signal if deployed for MPE systems. To resolve the PE, however, multiple GRSs are employed. In an MLAT system, a minimum of 3 GRSs is required while the MPE system requires only a minimum of 2 [12].

2.1. Problem statement

Factors that affect the accuracy of target positioning among others are the range between the receiving station and target, transmit power, antenna gain, frequency, and receiver sensitivity. The signal in the form of electromagnetic emission of the target, which may be a radar or communication signal, is transmitted over a distance and received at the GRS antenna. As the target moves further apart in range, the value of the SNR falls. This raises the noise level and therefore introduces error in the measured AOA. The error in the AOA estimate is passed on to the angulation algorithm that processes the AOA estimate. Overall, the increase in the noise level as a result of lower SNR contributes significantly to the higher PE error.

The antenna arrangement used in the GRS, which may be linear or a circular array configuration, significantly affects the coverage of the AOA estimation. The linear array exhibits the left-right ambiguity in the AOA estimate while the circular array offers 360° azimuthal coverage but is associated with rank-1 ambiguity [21]. Rank-1 ambiguity is caused by parasite peaks in the spectrum due to high-level side lobes in the antenna beam pattern, which creates difficulty in differentiating two closely spaced bearings, θ_1 and θ_2 [22, 23].

In this paper, the method employed for AOA estimation of the MPE system is assumed to be uniformly distributed over all bearings. Preliminary work in [24] showed that the distribution of the coefficient matrix condition number and PE errors do not appear to be uniformly distributed over all fields of coverage. Instead, the error appears higher within 80° to 100° and 260° to 280° fields of coverage. This paper will therefore be focused on the PE error due to the angulation process and investigate the correlation that exists between the PE error and the condition number of the coefficient matrix as well as the effect of GRS placement error on the PE accuracy of the MPE system.

2.2. Angulation algorithm description

This section presents the angulation theory and the mathematical derivations that describe the MPE system. Figure 1 illustrates the 2-stage process involved in position estimation using a 4-GRS square layout MPE system. At the input stage, the receiver estimates the AOA, which is the PDSP used as input at stage 1. Next, the angulation algorithm at stage 2 estimates the target PE by using the PDSP estimated from stage 1 with reference to the coordinate information of the GRS. The result of the estimation is displayed at the output for further action.

2.3. Angulation algorithm position estimation

Let θ_i be the AOA of the target in radians located at (x, y) obtained at the ith GRS with coordinates (x_i, y_i) in Figure 2. The figure represents multiple GRSs employed for target PE based on a 2-D 4-GRS square configuration with side length of 2.5 km. The GRSs are identified as GRS-1, GRS-2, GRS-3, and GRS-4 with coordinates $(x_1, y_1), (x_2, y_2), (x_3, y_3)$, and (x_4, y_4), respectively. The respective AOAs received at those GRSs are $\theta_1, \theta_2, \theta_3$, and θ_4.

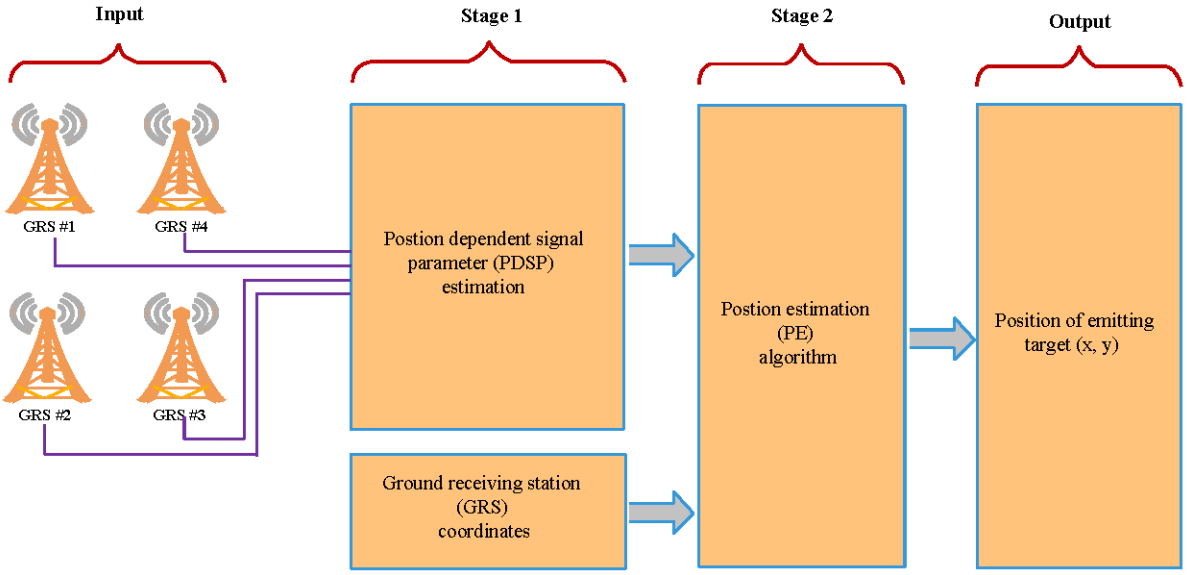

Figure 1. MPE system PE process [9].

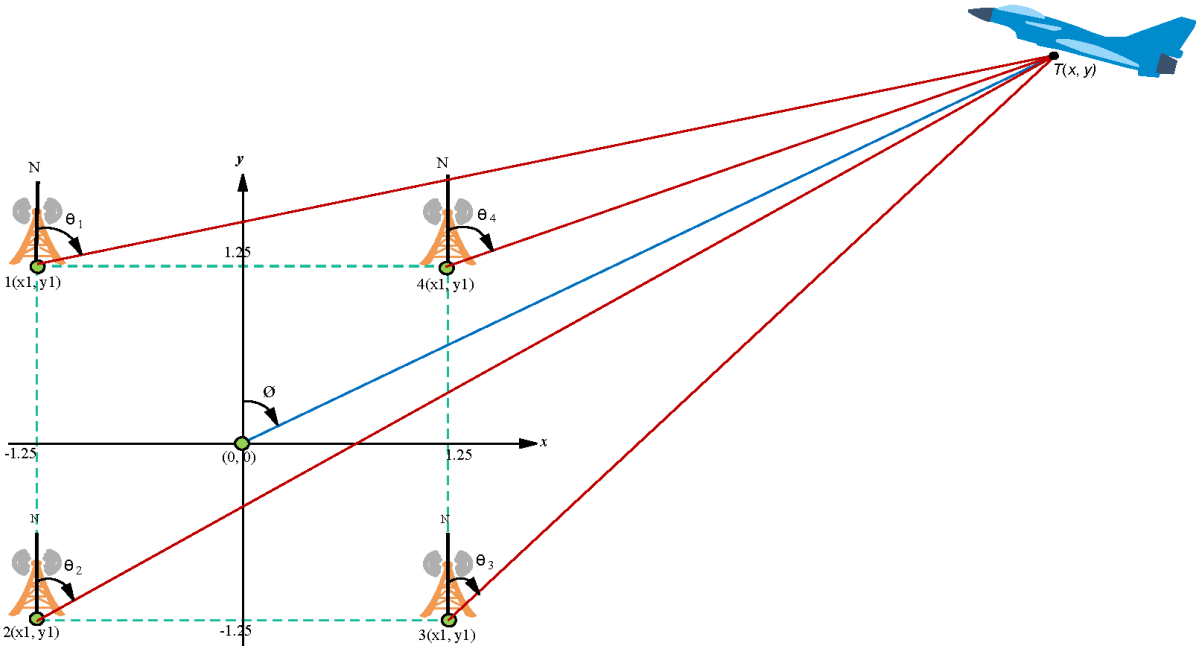

Figure 2. MPE system arrangement.

The central processing system (CPS), which constitutes the receiver and other processing hardware, is situated at the reference center with coordinates $(0,0)$ while the target is located at coordinates (x,y) with bearing ϕ. The AOA of the signal at the ith GRS, θ_i, is first to be determined, which may be through any of the classical methods like correlative interferometry and beamforming or advanced resolution techniques like MUSIC and ESPRIT [17, 25]. The computed AOA is corrupted by noise in the received signal, which therefore results in AOA error $e_{\theta i}$ at any ith GRS. This is modeled using Gaussian distribution [26] with zero mean

and standard deviation, σ, based on a widely used assumption in many localization algorithms [27]. Since the GRSs are of similar specification, the standard deviations (SDs) are the same for each receiver and the notation σ_θ is used instead of $e_{\theta i}$ for the SD. The estimated AOA, ϑ_i, expressed in terms of the actual AOA, θ_i and the AOA error SD, σ_θ is given as [9]:

$$\vartheta_i = \theta_i + e_{\theta i}. \tag{1}$$

The relationship between the GRS coordinates and the actual AOA, θ_i, is linear and is expressed by the following line-of-bearing (LOB) equation [9]:

$$y = m_i x + c_i, \tag{2}$$

where m_i is the gradient and c_i is the y-axis intercept expressed in terms of the AOA error, given as follows [9, 28]:

$$m_i = tan(\theta_i + e_{\theta i}), \tag{3}$$

$$c_i = y_i - x_i + tan(\theta_i + e_{\theta i}). \tag{4}$$

By substitution and rearranging (1) to (4), a set of 4 LOB equations with 2 unknowns are formed as follows [28]:

$$\left.\begin{array}{l} y = xtan(\theta_1 + e_{\theta 1}) - x_1 tan(\theta_1 + e_{\theta 1}) + y_1 \\ y = xtan(\theta_2 + e_{\theta 2}) - x_2 tan(\theta_2 + e_{\theta 2}) + y_2 \\ y = xtan(\theta_3 + e_{\theta 3}) - x_3 tan(\theta_3 + e_{\theta 3}) + y_3 \\ y = xtan(\theta_4 + e_{\theta 4}) - x_4 tan(\theta_4 + e_{\theta 4}) + y_4 \end{array}\right\}. \tag{5}$$

The set of LOB equations in (5) are trigonometrically represented as 4 straight lines whose solution $\boldsymbol{x}$ is their intersection [29]. This can be represented in matrix system in the following form:

$$\mathbf{A}\mathbf{x} = \mathbf{b}, \tag{6}$$

where the matrix $\mathbf{A}$ and the vector $\mathbf{b}$ are obtained from (5) and defined as follows [9, 17]:

$$\mathbf{A} = \begin{bmatrix} tan(\theta_1 + e_{\theta 1}) & 1 \\ tan(\theta_2 + e_{\theta 2}) & 1 \\ tan(\theta_3 + e_{\theta 3}) & 1 \\ tan(\theta_4 + e_{\theta 4}) & 1 \end{bmatrix}, \ \mathbf{x} = \begin{bmatrix} x \\ y \end{bmatrix}, \ \mathbf{b} = \begin{bmatrix} y_1 + x_1 tan(\theta_1 + e_{\theta 1}) \\ y_2 + x_2 tan(\theta_2 + e_{\theta 2}) \\ y_3 + x_3 tan(\theta_3 + e_{\theta 3}) \\ y_4 + x_4 tan(\theta_4 + e_{\theta 4}) \end{bmatrix}. \tag{7}$$

For small angles, $tan(\theta_i + e_{\theta i})$ in (7) can be approximated as follows:

$$tan(\theta_i + e_{\theta i}) = tan(\theta_i) + e_{\theta i}. \tag{8}$$

Equation (8) is derived by applying trigonometric identity for summation of angles and the small angle approximation for tangent. Substituting (8) into (7) results in:

$$\mathbf{A} = \begin{bmatrix} tan(\theta_1) + e_{\theta 1} & 1 \\ tan(\theta_2) + e_{\theta 2} & 1 \\ tan(\theta_3) + e_{\theta 3} & 1 \\ tan(\theta_4) + e_{\theta 4} & 1 \end{bmatrix}, \ \mathbf{b} = \begin{bmatrix} y_1 + x_1 tan(\theta_1) + x_1 e_{\theta 1} \\ y_2 + x_2 tan(\theta_2) + x_2 e_{\theta 2} \\ y_3 + x_3 tan(\theta_3) + x_3 e_{\theta 3} \\ y_4 + x_4 tan(\theta_4) + x_4 e_{\theta 4} \end{bmatrix}. \tag{9}$$

The matrix system in (9) has a greater number of equations than unknowns. Therefore, the equation $\mathbf{Ax} = \mathbf{b}$ is overdetermined and has no unique solution [30]. Matrix $\mathbf{A}$ can be converted to a square matrix by multiplying both sides of (6) with its transpose, $\mathbf{A}^{\mathrm{T}}$. Due to the error, $e_{\theta i}$, which is a random variable, the estimated position $\mathbf{x}$ has to be resolved for all possible realizations. Applying the expectation operation on both sides of the system in (9), the modified LOB equation where $\mathbf{A}^{\mathrm{T}}\mathbf{A}$ is the modified coefficient matrix and $\mathbf{A}^{\mathrm{T}}\mathbf{b}$ is the modified constant vector is thus given as:

$$E[\mathbf{A}^{\mathrm{T}}\mathbf{A}]\mathbf{x} = E[\mathbf{A}^{\mathrm{T}}\mathbf{b}]. \tag{10}$$

Many methods to compute the matrix inverse such as Gaussian elimination, LU decomposition, or least squares (LS) estimation may be used to find the solution to (10). The solution to the estimation based on matrix inversion can be expressed as follows:

$$E[\mathbf{x}] = E[(\mathbf{A}^{\mathrm{T}}\mathbf{A})^{-1}\mathbf{A}^{\mathrm{T}}\mathbf{b}]. \tag{11}$$

We therefore choose the singular value decomposition (SVD) to find the solution to the LS problem in (11). The SVD, among other advantages, enables the solution to be found for nonsymmetrical matrix systems. It also provides the eigenvalues and eigenvectors and, as well, allows dimensionality reduction, which has the benefit of reducing storage space, speeding computation, and eliminating redundant elements [31, 32]. Referring to (10), the SVD can be obtained for the LHS of the equation by:

$$E[\mathbf{A}^{\mathrm{T}}\mathbf{A}] = E[\mathbf{U}\Sigma\mathbf{V}^{\mathrm{T}}], \tag{12}$$

where the matrix $\mathbf{A}^{\mathrm{T}}\mathbf{A} \in \mathbb{C}^{m\times n}$ is decomposed into products of three matrices as in (12), such that $\mathbf{U} \in \mathbb{C}^{m\times m}$ and $\mathbf{V} \in \mathbb{C}^{n\times n}$ are unitary matrices while Σ is a diagonal matrix with the same shape as $\mathbf{A}^{\mathrm{T}}\mathbf{A}$ having nonnegative entries. Since $\mathbf{A}^{\mathrm{T}}\mathbf{A} = \mathbf{U}\Sigma\mathbf{V}^{\mathrm{T}}$, the modified system matrix on the LHS of (10) containing the estimated AOA, θ_i, and the AOA error, $e_{\theta i}$, can now be expressed in terms of the components of the SVD. Thus,

$$E\{[\mathbf{U}\Sigma\mathbf{V}^{\mathrm{T}}]\mathbf{x}\} = E[\mathbf{A}^{\mathrm{T}}\mathbf{b}]. \tag{13}$$

The position $\boldsymbol{x}$ is estimated by:

$$E[\mathbf{x}] = E\{[\mathbf{U}^{\mathrm{T}}\Sigma^{-1}\mathbf{V}]\mathbf{A}^{\mathrm{T}}\mathbf{b}\}. \tag{14}$$

With reference to (13), the first step involves evaluating the LHS. This enables us to derive the coefficient matrix condition number while the RHS of the same equation is used when we want to estimate the PE error as expressed by (14). The elements $\mathbf{A}_{i,j}(i,j=1,2)$ are obtained by taking the expectation on each element in matrix $\mathbf{A}^{\mathrm{T}}\mathbf{A}$.

3. Position estimation error analysis

This section analyzes how the AOA error, $e_{\theta i}$, caused by noise in the AOA estimation affects the accuracy of the multiangulation process. We start by simplifying the terms in (12) and (13), whose results are then used to calculate the condition number, $k[\mathbf{A}^{\mathrm{T}}\mathbf{A}]$, which is in turn linked to the PE error analysis. The expectation

operation significantly simplifies the modified coefficient matrix $\mathbf{A}^{\mathrm{T}}\mathbf{A}$ as well as the modified constant vector $\mathbf{A}^{\mathrm{T}}\mathbf{b}$. The resulting modified coefficient matrix is written as:

$$E[\mathbf{A}^{\mathrm{T}}\mathbf{A}] = E\begin{bmatrix} a_{11} & a_{12} \\ a_{21} & a_{22} \end{bmatrix} = \begin{bmatrix} E[a_{11}] & E[a_{12}] \\ E[a_{21}] & E[a_{22}] \end{bmatrix}. \tag{15}$$

The derivation of (15) follows from taking the expectation to simplify the result of the product of the two matrices $\mathbf{A}^{\mathrm{T}}$ and $\mathbf{A}$. The elements of $\mathbf{A}^{\mathrm{T}}\mathbf{A}$, after the expectation operator is applied, are as follows:

$$E[a_{11}] = \sum_{i=1}^{4} tan(\theta_i)^2 + 4\sigma_e^2, \tag{16}$$

$$E[a_{12}] = E[a_{21}] = \sum_{i=1}^{4} tan(\theta_i). \tag{17}$$

$$E[a_{22}] = 4. \tag{18}$$

Only $E[a_{11}]$, among all the elements of $E[\mathbf{A}^{\mathrm{T}}\mathbf{A}]$, contains the variance, σ_e^2 of the AOA error. The diagonal elements $E[a_{12}]$ and $E[a_{21}]$ are the same and contain only the AOA information, θ_i, while element $E[a_{22}]$ is a constant term. By evaluating the RHS of (13) also, the elements $b_i(i = 1, 2)$ are obtained by taking the expectation on each element in $\mathbf{A}^{\mathrm{T}}\mathbf{b}$. The result of the expectation simplifies the equation as follows:

$$E[\mathbf{A}^{\mathrm{T}}\mathbf{b}] = E[\begin{bmatrix} b_1 \\ b_2 \end{bmatrix}] = \begin{bmatrix} E[b_1] \\ E[b_2] \end{bmatrix}. \tag{19}$$

Derivation of (19) follows the same procedure as derivation of (15). The elements of $\mathbf{A}^{\mathrm{T}}\mathbf{b}$ after the expectation operator is applied are as follows:

$$E[b_1] = \sum_{i=1}^{4} y_i tan(\theta_i) + \sum_{i=1}^{4} x_i tan(\theta_i)^2 + 4\sigma_e^2 \sum_{i=1}^{4} x_i, \tag{20}$$

$$E[b_2] = \sum_{i=1}^{4} y_i + \sum_{i=1}^{4} x_i tan(\theta_i). \tag{21}$$

It can be observed that among the elements of $E[\mathbf{A}^{\mathrm{T}}\mathbf{b}]$, only $E[b_1]$ contains the variance σ_e^2 of the AOA error. Other terms containing the AOA, θ_i, and the coordinates information of the GRS, x_i and y_i, appear both in $E[b_1]$ and $E[b_2]$. At higher SNR values, the AOA error SD, $e_{\theta,i} \approx 0$, eliminates the noise variance in (16) and (20). This reduces (16) to contain only the AOA squared term while (20) contains the x and y coordinates and the AOA squared term as well.

The condition number $k[\mathbf{A}^{\mathrm{T}}\mathbf{A}]$, in general, measures the sensitivity of the LOB equations to error [33]. If small errors in the coefficients or in the solution process have only a minor effect on the solution, the LOB equation is well conditioned; otherwise, it is ill conditioned [33]. The coefficient matrix condition number $k[\mathbf{A}^{\mathrm{T}}\mathbf{A}]$ is used to correlate with the PE error distribution of the multiangulation system through the analysis

of the eigenvalues of the coefficient matrix. Since SVD is used to determine the solution shown in (11), the singular values obtained can be used to determine the condition number without additional computation. The process for generating the SVD begins with estimating the singular matrix, Σ, followed by the computation of the eigenvector $\mathbf{V}$ and then subsequently the unitary matrix $\mathbf{U}$ [31]. The eigenvalue is related to the singular values defined as follows:

$$\lambda_n = \sqrt{\mathbf{s}_n}, \tag{22}$$

where $\boldsymbol{s}_n$ is the nth singular value. The matrix of the singular values for the given 2-by-2 system of equation is presented as follows:

$$\Sigma = \begin{bmatrix} s_1 & 0 \\ 0 & s_2 \end{bmatrix}. \tag{23}$$

The eigenvalues can be obtained by solving the equation of the modified coefficient matrix:

$$E[(\mathbf{A}^{\mathrm{T}}\mathbf{A}) - \lambda\mathbf{I}]\mathbf{x} = 0. \tag{24}$$

Solving for the determinant in (24) provides the eigenvalues. Using the solution to the quadratic equation,

$$\lambda = \frac{1}{2}(a_{11} + a_{22}) \pm \frac{1}{2}\sqrt{(a_{11} + a_{22})^2 - 4(a_{11}A_{22} - a_{12}a_{21})}, \tag{25}$$

and substituting in (25) the values of a_{11}, a_{12}, a_{21}, and a_{22} obtained from (16) to (18) provides the values of λ_1 and λ_2. Hence, the coefficient matrix condition number $k[\mathbf{A}^{\mathrm{T}}\mathbf{A}]$ computed for $\lambda_i (i = 1, 2)$ is obtained by the ratio of the two eigenvalues as follows:

$$k[\mathbf{A}^{\mathrm{T}}\mathbf{A}] = max(\lambda_1/\lambda_2), \tag{26}$$

or

$$k[\mathbf{A}^{\mathrm{T}}\mathbf{A}] = max(\lambda_2/\lambda_1). \tag{27}$$

4. Simulation results

This section discusses first the parameters of the wireless propagation model selected, the AOA estimation (correlative interferometry), the wireless data link, and the GRS setup parameters required to run the simulation. Next, a comparison is made between the condition number and the PE error. Simulation results cover the variation of the received SNR versus the target range, AOA error standard deviation versus the SNR, and the coefficient matrix condition number and PE error.

4.1. Simulation parameters

In real applications, as the target goes far in range, the SNR reduces, resulting in increased AOA error standard deviation. To verify this, the free-space wireless propagation channel is used to establish the relationship between the AOA error standard deviation and the target range. The signal transmitted is assumed from an UAS flying at 400 ft altitude with low transmit power, which may either be from an onboard radar or wireless data link. For this evaluation, the wireless data link parameters used were those allocated by the MCMC in Table 1 for frequency assignment and maximum equivalent isotropically radiated power (EIRP) [34].

Table 1. Wireless data link parameters by MCMC [34].

No.	Radio frequency (MHz)	Max. EIRP
1	433–435	100 mW
2	2400–2500	500 mW
3	5725–5875	1 W

Because of the low-altitude consideration and the existence of an unobstructed line of sight (LOS) between the target and the GRS antennas, the free-space path loss (FSPL) propagation model is selected to characterize the link between them. The FSPL attenuation of the received signal at the ith GRS in dB is given as:

$$L_{FS,i} = 32.44 + 20log_{10}d_i + 20log_{10}f_c + L_s, \tag{28}$$

where d_i is the target-to-GRS distance in km, f_c is the carrier frequency of the signal in MHz, and L_s is the cabling connector and other losses in dB. The received power in dBm at the ith GRS is expressed as:

$$P_{r,i} = P_t + G_t + G_r - L_{FS,i}, \tag{29}$$

where P_t is in dBm, and G_t and G_r are the transmit and receive antenna gain respectively in dBi. The SNR in dB is therefore calculated as follows:

$$SNR = P_{r,i} - S_n, \tag{30}$$

where S_n is the receiver sensitivity in dBm. Table 2 provides the parameters used to simulate the propagation channel [35].

Table 2. Parameters of wireless propagation channel.

No.	Parameter	Values
1	Transmit power	500 mW
2	Transmit antenna gain	3 dBi
3	Receive antenna gain	12 dBi
4	Carrier frequency	2.4 GHz
5	Receiver sensitivity	–90 bBm
6	Cabling and other losses	2 dB

The parameters in Table 1 and Table 2, which are based on the low altitude UAS, have boundaries defined by the MCMC and the Civil Aviation Authority of Malaysia. The former, in its Civil Aviation Regulations 2016 Part XVI Regulation 140, limits the UAS altitude to an allowable 400 ft maximum [36], while the latter regulates the link parameters between the UAS and the GRS. Since our assumption in this paper is that the target is an UAS that operates on a 2400 MHz link, the MCMC, based on its document 'Use of Frequencies for UAS', limits the transmit power for frequency of 2400 MHz to a maximum of 500 mW as shown in Table 1. Based on the UAS's altitude and the height of the GRS antenna, the maximum range R (km) that can achieve direct LOS communication, which depends on the earth's curvature as referenced in (11), is about 50 km. This can be shown using a mathematical formula as follows [37]:

$$D_{LOS} = 4.124\sqrt{h_1} + 4.124\sqrt{h_2}, \tag{31}$$

where D_{LOS} is the LOS distance, h_1 is the altitude of the transmitting target (122 m), and h_2 is the height of the GRS antenna (2m). Substituting the values gives $D_{LOS} = 4.124\sqrt{2} + 4.124\sqrt{122} = 51$ km.

To best receive the signal from the low-altitude UAS, it is desired to have high transmit power, high gain antenna, a receiver with very high sensitivity, and no-loss condition due to cabling connectors. The parameters defined in Table 1 and Table 2 are based on the following justifications: In reality, it is not possible to transmit high power because of the regulatory and practical considerations such as the use of limited transmit power by the UAS described earlier. Secondly, it may practically also incur cumbersome weight to the UAS due to large battery and other circuitry requirements. The values for antenna gains depend on application. The antenna on the UAS is omnidirectional to enable 360° coverage. Omnidirectional antennas have low gain, and in consideration of the size and weight constraints, we selected the antenna by L-com,[1] having a gain of 3 dBi, for this application. On the receiving side, the GRS antenna must be high-gain in order to maximize the received signal strength or the SNR performance from the transmitted weak signal [35] as related by (29) and (30). Since many UAS such as the DJI Matrice-200[2] operates based on a Wi-Fi spectrum of 2400 MHz, we assume that the receiver parameters follow Wi-Fi specifications. Based on these, the ANOM2412[3] antenna with a gain of 12 dBi is selected. A high sensitivity receiver is therefore required at the GRS. Because a Wi-Fi receiver is assumed, a receiver with a very high sensitivity of –91 dBm described in [38] is selected. In our calculation, –90 dBm is used only for convenience as in the previous work reported in [9] and [39].

4.2. Estimation of AOA error standard deviation with target range

Using the information in Table 1 and Table 2, the FSPL model was simulated in order to show the relationship between the target range, AOA error SD, and the received SNR and how they affect the AOA estimation. There are many methods used to perform AOA estimation, such as those highlighted in Section 2.3. The correlative interferometry based on an 8-element linear array such as the one used in [40] is employed here to assess the relationship between the AOA error SD and the range for a given transmit power. The relationship obtained is then used in the angulation algorithm to compute the PE. Based on Table 1, the target is assumed to use a carrier frequency of 2.4 GHz and transmit power of 500 mW, placed at bearing of $\pi/4$ radians (45°). The variations of the received SNR with the target azimuthal range and the variation of the SD with the SNR based on 100 runs of Monte Carlo simulation are shown in Figures 3a and 3b.

It can be observed from Figure 3a that the SNR degrades with target range because of attenuation. At a range close to the GRS, the SNR is high at about 35 dB and decreases beyond 33 km. As the SNR decreases with target range, the AOA error SD also decreases, as shown in Figure 3b. Thus, it can be seen that the SNR depends on the target horizontal range, which in turn affects the AOA error SD.

4.3. Multiangulation azimuthal PE error and condition number

The simulation parameters and the results obtained from the simulations are presented in this section. A target azimuth range of 1 km to 50 km with bearing of 0° to 360° and GRS spacing of 2.5 km were considered for the simulations of condition number and the PE error. The AOA error SD required to model the normal distribution is acquired from the estimation in Section 4.2 (Figure 3b).

[1]L-com. Dual band omni antenna [online]. https//www.l-com.com/wireless-antenna-24-ghz-900-mhz-3-dbi-dual-band-omni-antenna-nmo-connector [accessed 5 Dec. 2019].

[2]DJI Technology Inc. MATRICE 200 Series [online]. https://www.dji.com/matrice-200-series/info. [accessed: 10 Dec. 2019].

[3]AIR802. ANOM2412 Wi-Fi outdoor omnidirectional [online]. https//www.air802.com/antenna-wifi-omni-directional-2.4-ghz-12-dbi-outdoor-mast-mount.html [accessed 2 Dec. 2019].

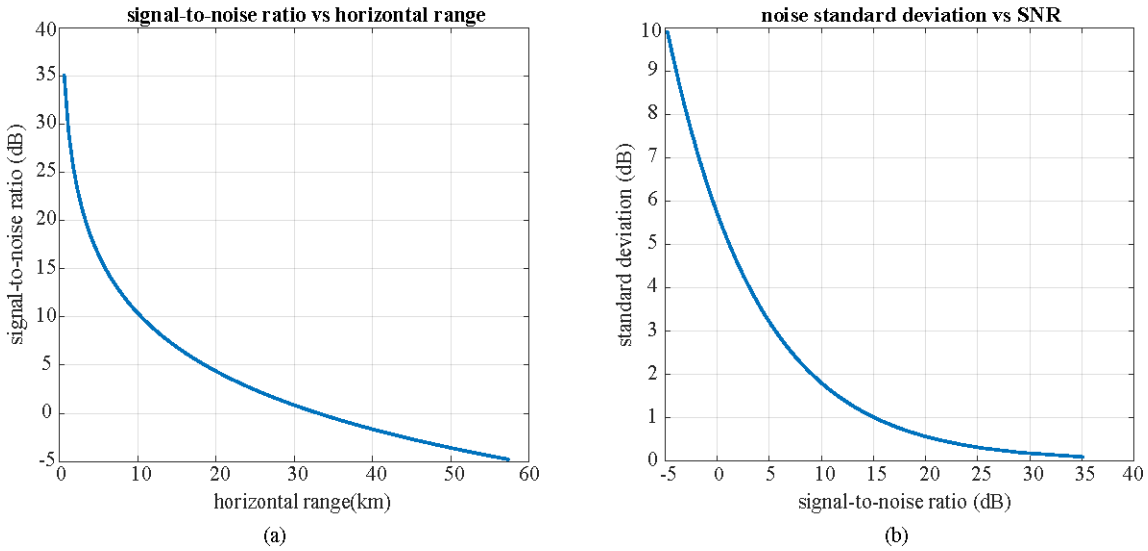

Figure 3. Relationship between SNR, AOA error SD, and target range: (a) SNR versus target range, (b) AOA error SD versus SNR.

The performance is measured in terms of the root mean square error (RMSE) between the actual and estimated target positions calculated for various target position and bearing. The mathematical expression for the RMSE for the N-run Monte Carlo simulation is given as:

$$RMSE = \sqrt{\frac{1}{N}\sum_{i=1}^{N}[(\hat{x}_i - x)^2 - (\hat{y}_i - y)^2]}, \tag{32}$$

where (x, y) and $(\hat{x}_i,\ \hat{y}_i)$ for $i = 1$ to 4 are the actual and the estimated position coordinates of the target, respectively.

4.3.1. Correct placement of GRS

A 4-GRS square layout as shown in Figure 4 with a separation distance of 2.5 km is adopted. This layout is chosen for its simplicity and convenience due to its symmetry, which enables results in one quadrant to be applied to other quadrants [11].

Figure 5 shows the contour plots of the coefficient matrix condition number and the azimuthal coordinate PE RMSE distributions based on the variation of the AOA error SD with target range estimated in Section 4.2 (illustrated in Figure 3b). It can be seen also from the plots that both the condition number and the target azimuthal coordinate PE RMSE in Figure 5a and Figure 5b increase with the target range from 1 km to 50 km. Both appear to be roughly uniform within the same range and bearings such as above 100° to about 260° and above 280° to about 80°. However, they vary greatly within the bearings of 80° to 100° and 260° to 280°. For instance, a condition number and PE error values of 1827 and 1.56 occur at the range of 50 km and bearing of 90°, respectively. A slight change in the range to 49.2 km and the bearing of 84.9° causes the condition number to rise to 2425 and the PE error dropped to 0.62. Similarly, this is true for a slight change in the range and bearing of 40 km and 90° to 39.9 km and 85°, the condition number and PE error values of 1169 and 0.86 changed to 1847 and 0.33 respectively. Thus, there is a relationship between condition number and PE error at various ranges and bearings.

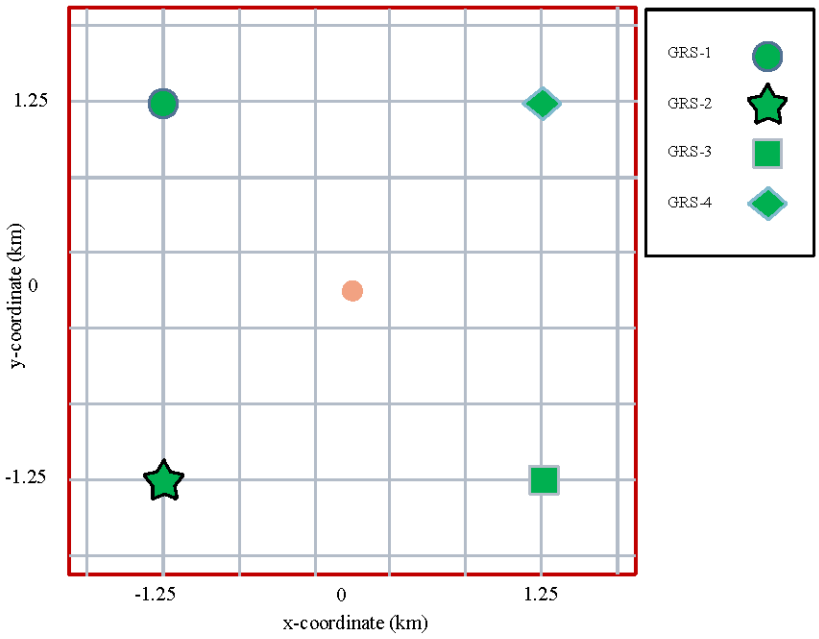

Figure 4. 4-GRS square layout.

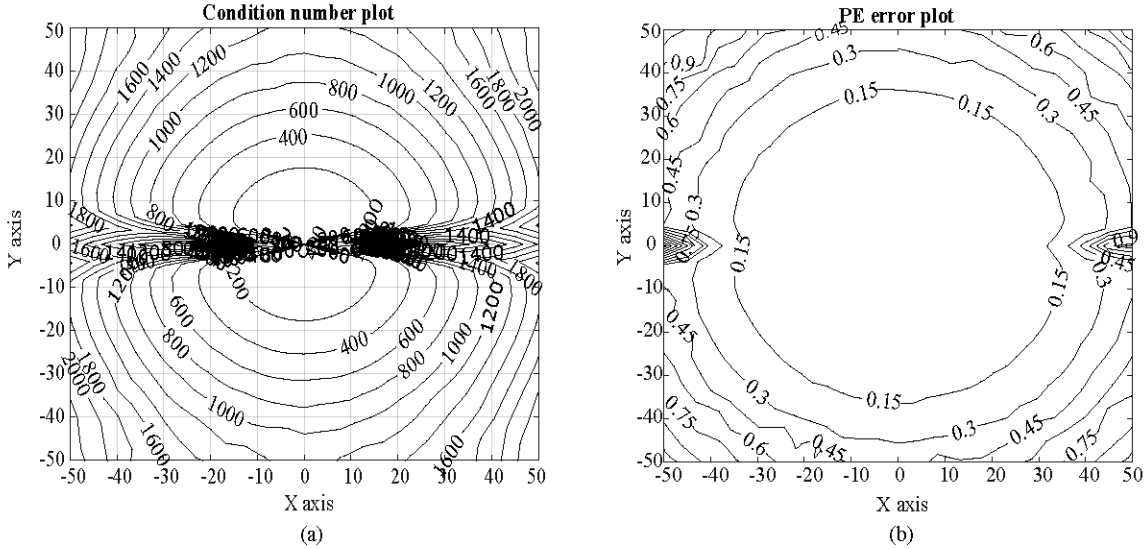

Figure 5. Condition number and RMSE distribution for target range of 0 km to 50 km and bearing coverage of 0° to 360° using 2.5 km GRS separation: (a) condition number $k[\mathbf{A}^{\mathrm{T}}\mathbf{A}]$ distribution, (b) PE RMSE distribution.

4.3.2. Incorrect placement of GRS

This section describes distortion and loss of symmetry in the distribution of the condition number and PE error due to the GRS misplacement. To show this effect, two GRSs (GRS-1 and GRS-4) are selected as shown in Figure 6a and Figure 6b.

In Figure 6a, for instance, GRS-1 (coordinates: –1.25, 1.25) is erroneously misplaced (coordinates: –1.5, 0.25), while the remaining three GRSs are assumed correctly placed. Due to this effect, the plots of the condition number and PE error appear distorted as shown in Figure 7a and Figure 7b, respectively.

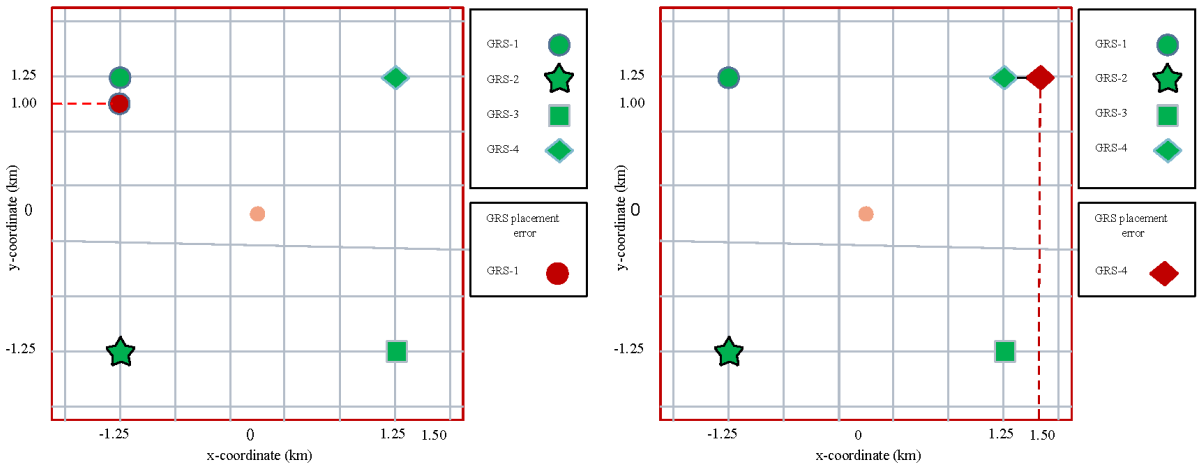

Figure 6. 4-GRS square layout with misplacement error: (a) misplacement error at GRS-1, (b) misplacement error at GRS-4.

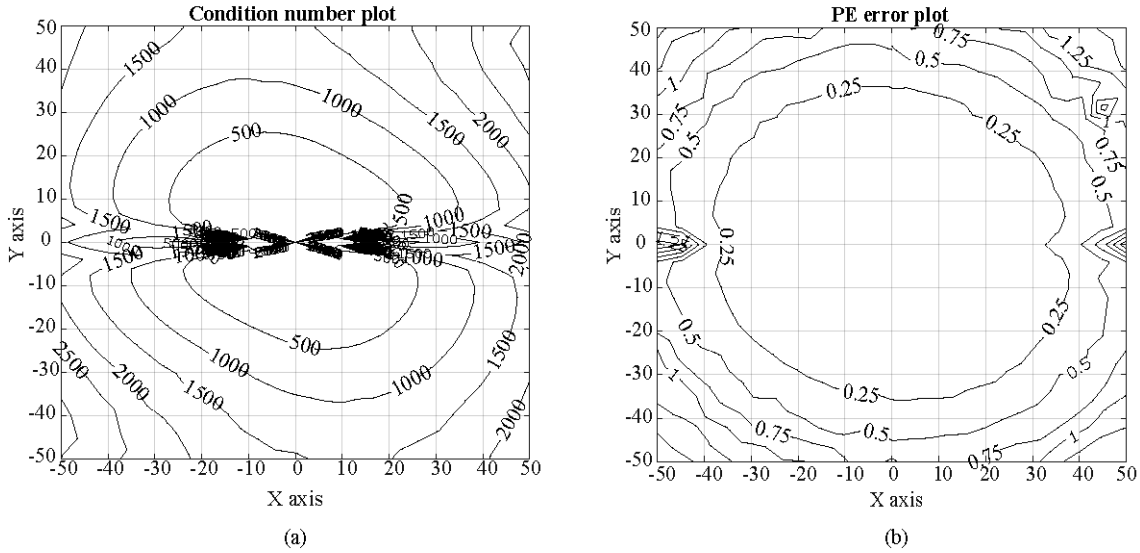

Figure 7. Effect of misplacement error at GRS-1: (a) distorted condition number $k[\mathbf{A}^{\mathrm{T}}\mathbf{A}]$ distribution, (b) distorted PE RMSE distribution for target range of 0 km to 50 km and bearing coverage of 0° to 360°.

Similarly, in Figure 6b, GRS-4 (coordinates: 1.25, 1.25) is erroneously misplaced (coordinates: 1.5, 1.25), with the other three GRSs assumed correctly placed. Due to this effect, the plots of the condition number and PE error appear also distorted as shown in Figure 8a and Figure 8b, respectively.

The plots of Figures 7a and 7b and Figures 8a and 8b show bent contour distribution for both the condition number and the PE RMSE distribution, respectively. In Figure 7, for instance, by alternating the same placement error to an opposite GRS, i.e. GRS-4 (coordinates: 1.25, 1.25), incorrectly misplaced (coordinates: 1.5, 0.25), the axis of the distorted shape changes as in Figures 8a and 8b. The nonuniformity simply shows the effect of GRS placement error on the two respective distributions. This shows that the shape of the distribution depends on for which GRS exactly the misplacement error occurs. Furthermore, the results

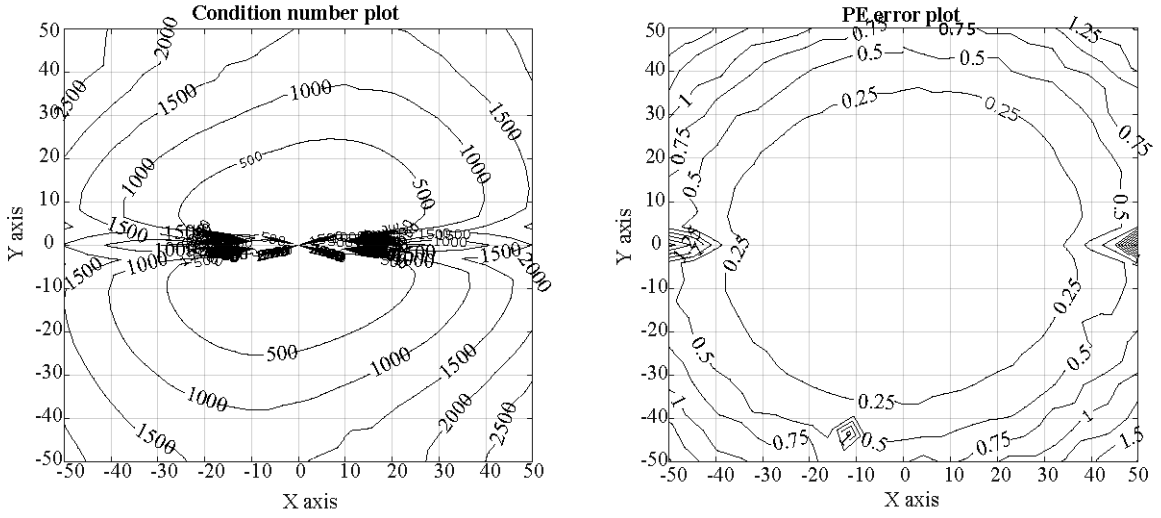

Figure 8. Effect of misplacement error at GRS-4: (a) distorted condition number $k[\mathbf{A}^{\mathrm{T}}\mathbf{A}]$ distribution, (b) distorted PE RMSE distribution for target range of 0 km to 50 km and bearing coverage of 0° to 360°.

obtained for condition number, assuming correct placement of GRSs such as in Figure 5a in Section 4.3.1, can enable us to predict or have an idea of the nature of the distribution of the PE error in Figure 5b. By comparing this, on the other hand, to the condition number distribution for incorrect GRS placement in Section 4.3.2 such as in Figure 7a, it will be difficult to make a reasonable prediction on the distribution of the PE error because of the distorted nature of the distribution due to the placement error.

5. Conclusion

Error in AOA estimation caused by noise in the received signal subsequently leads to PE error in a multiangulation system. The proposed approach in this paper is based on mathematical derivations to arrive at the condition number of the coefficient matrix and the PE error of the multiangulation system via SVD-based eigenvalue approach and expectation operations. The main objective is to prove and establish the correlation that exists between the condition number of the coefficient matrix and the PE and use the information to assess the sensitivity of the angulation PE error. This approach, to the best of our knowledge, has not been previously investigated by any researchers. The LS estimation is first performed on the matrix representation of the LOB equations. Simplification is first performed by taking the expectation of the LOB equation followed by the SVD computation to obtain the condition number from the eigenvalues. A higher condition number means that the solution of the LS estimation is more sensitive to the computation error, leading to higher PE error. Analysis is performed to determine the effect of condition number and PE error for a 4-GRS square configuration MPE system with GRS spacing of 2.5 km covering a target range up to 50 km and bearing from 0° to 360°. The FSPL model is used with the assumption that the target operates at transmit power of 500 mW and operating frequency of 2400 MHz. The results, based on Monte Carlo simulations, have shown that both condition number and PE error distribution increase with the target range. The distribution of the condition number and the PE error is uniformly distributed except at the bearings of 80° to 110° and 260° to 280°, where both are highly sensitive to slight changes in range and bearing, thereby indicating the direct correlation between the two parameters.

References

[1] Poisel R. Electronic Warfare Target Location Methods. Boston, MA, USA: Artech House, 2012.

[2] Bagheri M, Sedaaghi MH. A new approach to pulse deinterleaving based on adaptive thresholding. Turkish Journal of Electrical Engineering & Computer Sciences 2017; 25 (5): 3827-3838. doi: 10.3906/elk-1606-415

[3] Ayazgok S, Erdem C, Ozturk MT, Orduyilmaz A, Serin M. Automatic antenna scan type classification for next-generation electronic warfare receivers. IET Radar, Sonar & Navigation 2018; 12 (4): 466-474. doi: 10.1049/iet-rsn.2017.0354

[4] Lambert G. Electronic Warfare: Rethinking the Importance of Its Role in the Military Operations. Norfolk, VA, USA: Marine Corps, Joint Forces Staff College, National Defense University, 2016.

[5] Boyacı A, Ekti AR, Yarkan S, Aydın MA. Monitoring, surveillance, and management of the electromagnetic spectrum: current issues in electromagnetic spectrum monitoring. Electrica 2018; 18 (1): 100-108. doi: 10.5152/iu-jeee.2018.1816

[6] ITU Radiocommunication Sector (ITU-R). Handbook on National Spectrum Management, 2015.

[7] Pace PE. Detecting and Classifying Low Probability of Intercept Radar. 2nd ed. Boston, MA, USA: Artech House, 2009.

[8] Poisel RA. Introduction to Communication Electronic Warfare Systems. 2nd ed. Boston, MA, USA: Artech House, 2008.

[9] Sha'ameri AZ, Yaro AS, Amjad FM, Hamdi MN. Performance comparison of emitter locating system for low level airborne targets. Defence S and T Technical Bulletin 2017; 10(3): 199-217.

[10] Hassanhosseini S, Taban MR, Abouei J. Indoor localization of wireless emitter using direct position determination and particle swarm optimization. Turkish Journal of Electrical Engineering & Computer Sciences 2018; 26 (2): 655-665. doi: 10.3906/elk-1706-332

[11] Fard HT, Atashbar M, Norouzi Y, Kashani FH. Multireference TDOA-based source localization. Turkish Journal of Electrical Engineering & Computer Sciences 2013; 21 (Suppl. 1): 1920-1929. doi: 10.3906/elk-1109-46

[12] International Civil Aviation Organisation (ICAO). Guidance Material on Comparison of Surveillance Technologies (GMST), 2007.

[13] Norouzi Y, Kashani ES, Ajorloo A. Angle of arrival-based target localisation with low earth orbit satellite observer. IET Radar, Sonar & Navigation 2016; 10 (7): 1186-1190. doi: 10.1049/iet-rsn.2015.0437

[14] Series S. Comparison of Time-Difference-of-Arrival and Angle-of-Arrival Methods of Signal Geolocation, 2011.

[15] Sha'ameri AZ, Shehu YA, Asuti W. Performance analysis of a minimum configuration multilateration system for airborne emitter position estimation. Defence S and T Technical Bulletin 2015; 8 (1): 27-41

[16] Çelĩk G, Çelebi H, Partal HP, Zeydan E, Karatepe IA et al. An experimental study of indoor RSS-based RF fingerprinting localization using GSM and Wi-Fi signals. Turkish Journal of Electrical Engineering& Computer Sciences 2017; 25 (4): 2727-2736. doi: 10.3906/elk-1601-94

[17] Werner J, Wang J, Hakkarainen A, Gulati N, Patron D et al. Sectorized antenna-based DoA estimation and localization: Advanced algorithms and measurements. IEEE Journal on Selected Areas in Communications 2015; 33 (11): 2272-2286. doi: 10.1109/JSAC.2015.2430292

[18] Şahin S, Baba A, Sonmez T. Optimal fusion of multiple GNSS signals against spoofing sources. Turkish Journal of Electrical Engineering & Computer Sciences 2017; 25 (4): 3289-3299. doi: 10.3906/elk-1604-123

[19] Boashash B. Time-Frequency Signal Analysis and Processing: A Comprehensive Reference. San Diego, CA, USA: Academic Press, 2015.

[20] Kanaa A, Sha'ameri AZ. A robust parameter estimation of FHSS signals using time–frequency analysis in a non-cooperative environment. Physical Communication 2018; 26: 9-20. doi: 10.1016/j.phycom.2017.10.013

[21] Xiao W, Xiao XC, Tai HM. Rank-1 ambiguity DOA estimation of circular array with fewer sensors. In: IEEE 2002 45th Midwest Symposium on Circuits and Systems; Tulsa, OK, USA; 2002. pp. 29-32. doi: 10.1109/MWSCAS.2002.1186962

[22] Flieller A, Larzabal P, Clergeot H. Study of ambiguities in array manifold: A general framework. In: IEEE Proceedings of 8th Workshop on Statistical Signal and Array Processing; New York, NY, USA; 1996. pp. 574-577. doi: 10.1109/SSAP.1996.534942

[23] Tan KC, Goh SS, Tan EC. A study of the rank-ambiguity issues in direction-of-arrival estimation. IEEE Transactions on Signal Processing 1996; 44 (4): 880-887. doi: 10.1109/78.492541

[24] Yarima SM, Sha'ameri AZ, Yaro AS. Position estimation error and condition number correlative analysis of a multiangulation system. In: 7th International Graduate Conference on Engineering, Science and Humanity; Johor Bahru, Malaysia; 2018. pp. 338-340.

[25] Yan F, Jin M, Qiao X. Low-complexity DOA estimation based on compressed MUSIC and its performance analysis. IEEE Transactions on Signal Processing 2013; 61 (8): 1915-1930. doi: 10.1109/TSP.2013.2243442

[26] Goldsmith A. Wireless Communications. New York, NY, USA: Cambridge University Press, 2005.

[27] Wang C, Qi F, Shi G, Ren J. A linear combination-based weighted least square approach for target localization with noisy range measurements. Signal Processing 2014; 94: 202-211. doi: 10.1016/j.sigpro.2013.06.005

[28] Sand S, Dammann A, Mensing C. Positioning in Wireless Communications Systems. Chichester, UK: John Wiley & Sons, 2014.

[29] Kuçku K. Horizontal dilution of precision-based ultra-wideband positioning technique for indoor environments. Turkish Journal of Electrical Engineering & Computer Sciences 2014; 22 (5): 1307-1322. doi: 10.3906/elk-1301-20

[30] Strang G. Introduction to Linear Algebra, 4th ed. Wellesley, MA, USA: Wellesley-Cambridge Press, 2009.

[31] Hogben L. Handbook of Linear Algebra. Ames, IA, USA: Chapman and Hall/CRC, 2013.

[32] Abdurrazzaq A, Mohd I, Junoh AK, Yahya Z. A hybrid of tropical-singular value decomposition method for salt and pepper noise removal. Turkish Journal of Electrical Engineering & Computer Sciences 2019; 27 (3): 1667-79.

[33] Lay CD. Linear Algebra and Its Application. 3rd ed. Boston, MA, USA: Addison-Wesley Pearson Education Inc., 2012. doi: 10.1136/gut.44.2.e290

[34] Malaysian Communications and Multimedia Commission (MCMC). Use of Frequencies for Unmanned Aircraft Systems, 2015.

[35] SELEX Sistemi Integrati. ADS-B Subsystem: Standard E5010015201SDD, 2014.

[36] Civil Aviation Act 1969. P.U.(A), Civil Aviation Regulation 2016. Attorney General's Chambers of Malaysia.

[37] Straw RD. The ARRL Antenna Book. 21st ed. Newington, CT, USA: ARRL Inc., 2007.

[38] Datasheet Prolink PHA1010 v100. AP/CPE/Bridge/Repeater.

[39] Yaro AS, Sha'ameri AZ. Effect of path loss propagation model on the position estimation accuracy of a 3-dimensional minimum configuration multilateration system. International Journal of Integrated Engineering 2018; 10 (4): 1-20.

[40] Kamal SM, Adam AA, Ajagun AS. Performance evaluation of correlative interferometry for angle of arrival estimation. Journal of Emerging Trends in Engineering and Applied Sciences 2015; 6 (1): 43-48.